GBT Memo 323

An Ultrawideband Feed at Prime Focus: (0.7 – 4 GHz)

Steven White, Robert Simon, Laura Leyzorek

04/21/2026

Introduction

A dual polarization quad-ridged flared feed covering the frequency range 0.7 to 4 GHz is designed for the Green Bank Telescope prime focus, Figure 1-3. The motivation is improved pulsar timing for gravitational wave detection observed by the NanoGrav collaboration. In contrast to the pulsar observations where each pulsar has unique timing metrics, the receiver specification is characterized by a single parameter, total system temperature divided by efficiency, $\frac{T_{sys+(1-\eta_S)T_{gnd}}}{\eta_T}$. This parameter is optimized in a multi-step process where the CST Microwave Studio (CST MWS) time domain solver produces the electric far field pattern at specified frequencies.[12] The set of far field patterns is imported into a TICRA/GRASP model of the GBT that calculates the beam shape, spillover, $\boldsymbol{\eta_s}$, and total efficiency, $\boldsymbol{\eta_T}$.[6,11] The spillover is combined with both the measured and predicted component noise contributions from the atmospheric, galactic center and CMB to produce a total system temperature. When divided by GRASP total efficiency the value can be compared to the system equivalent flux density, SEFD, observations. The completion of the design required research efforts into quartz window fabrication and performance, along with challenging machining techniques of the complex curved three-dimensional ridge profiles. The details can be found in the files listing.

Design

The standard GBT feed horn is a hybrid design with a specified edge taper to produce an illumination of the reflector that optimizes antenna gain divided by total temperature. Two cylindrical waveguide modes, TE11 and TM11, are combined to give approximate linear electric field vectors at the aperture.[10] Although these feed horns produce well defined illumination characteristics with low cross polarization, the bandwidth upper to lower frequency ratio is limited to ~2:1 depending on the acceptable cross polarization. Increasing the bandwidth while maintaining a symmetrical illumination with low cross polarization requires additional first order azimuthal modes. Detailed design, analysis, and construction techniques are available in Akgiray and Beukman's theses. These are good references though achieving the Nanograv specification requires additional components and modifications complicating the analysis.[1,2] The modifications are the addition of a quartz spear to dielectric load the feed to improve the upper band response, a flared ridge design to reduce unwanted mode content, and extension of the feed section beyond the ridge end with a corrugated cone to reduce spillover at the lower band edge.[3] A thermal gap incorporated with a smaller diameter and thinner quartz fabric waveguide window located at ridge end reduces thermal loading. The CST MWS model with these components and feed dimensions of Figure 1 requires 650 million mesh cells making the computation time long and difficult to simulate and predict modal and cutoff frequencies, thus the optimization becomes a function of sheer number of model variations attempted, Files:1-4.

For the GBT offset design at prime focus, the effective focus to diameter ratio is 0.7. This ratio requires a feed with half angle beamwidth of 39 degrees with approximate diameter of 4 wavelengths at the lower band edge to give optimal illumination and spillover. At the shorter wavelengths of the upper band, the feed must combine additional cylindrical waveguide modes properly phased to increase illumination efficiency. The length of the feed primarily determines the beam illumination taper. Employing the analysis of Ludwig, an approximate feed pattern can be constructed that gives insight into the consequences of adding higher order modes to the beam shape and cross polarization; however, optimizing a particular mode content's amplitude and phase is a difficult time consuming task .[4] The electric field patterns produced by the CST MWS model can be deconstructed for modal content employing the same methods. The addition of higher order TE modes, TE12 and TE13, increase the illumination efficiency in the phi direction (H-plane) without changing the shape of the E-plane fields. Addition of higher order TM modes, TM12 and TM13, increase the illumination efficiency in the theta direction (E-plane) and do not affect the H-plane fields. The modal content is analyzed for the as built design and compared to the model without the spear. As Figures 2 indicates, slight changes in modal content give significant improvements in illumination and spillover efficiency.

The design procedure consists of first adjusting the ridge gap and width to maximize return loss, dimensions are shown in Figure 1. Also, the position of the quartz spear end relative to the probes is critical. With the parameters optimized for return loss fixed, the ridge and horn parameters can be adjusted to optimize efficiency and spillover. The input match improves by being differentially excited at impedance 100 Ohms. With limited time and budget, a differential amplifier was constructed of a Krytar commercial hybrid and a Low Noise Factor Amplifier. The amplifier has excellent noise properties; however, the gain begins to decrease at 3 GHz where the IF noise contribution begins to be significant. A Cosmic Microwave low noise amplifier was also tested that has a flat gain response greater than 4 GHz. The amplifier noise characteristic at the lower band where the flux of the pulsars increases nullified any benefit from the wider bandwidth. It is noted that the size and shape are constrained by the machining capabilities where the horn profile is z^p shown in Table 1:1, with the ridge profile being exponential, Table 1:2. Mechanical limitations of the GBT Sterling mount constrain the total size and weight. The ridge must be continuous to limit unwanted resonances and cryogenically cooled along with the amplifier and probe section.

The fabrication of the quartz window is well documented with experiments to ensure a safety margin for the atmospheric vacuum pressure differential that agreed with modeling results. Files:5. CST MWS models indicated that a window located at the feed aperture would adversely distort the far field patterns and reduce the return loss due to its size and increased thickness. Thus, the length of the ridges is limited by locating the window away from the aperture. Time and schedule did not allow time to experiment with either eliminating the gap or reducing the thickness. CST MWS models give better performance without a thermal gap, Figure 4. Measurements with the quartz dome installed, then repeated with the dome removed, agree with the model results as shown in Figure 8. The S-parameter model with measured S_{11} and setting S_{21}, S_{12} = 1 gives for the parameter

$$|\Gamma_{\mathrm{window}}|_{\mathrm{max}} < 0.170 \ (-15.39 \ \mathrm{dB})$$

$$\left|\Gamma_{feed+windo}\right| = \left|S_{11} + \frac{S_{12}S_{21}\,\Gamma_{window}}{1-S_{11}\Gamma_{window}}\right|$$

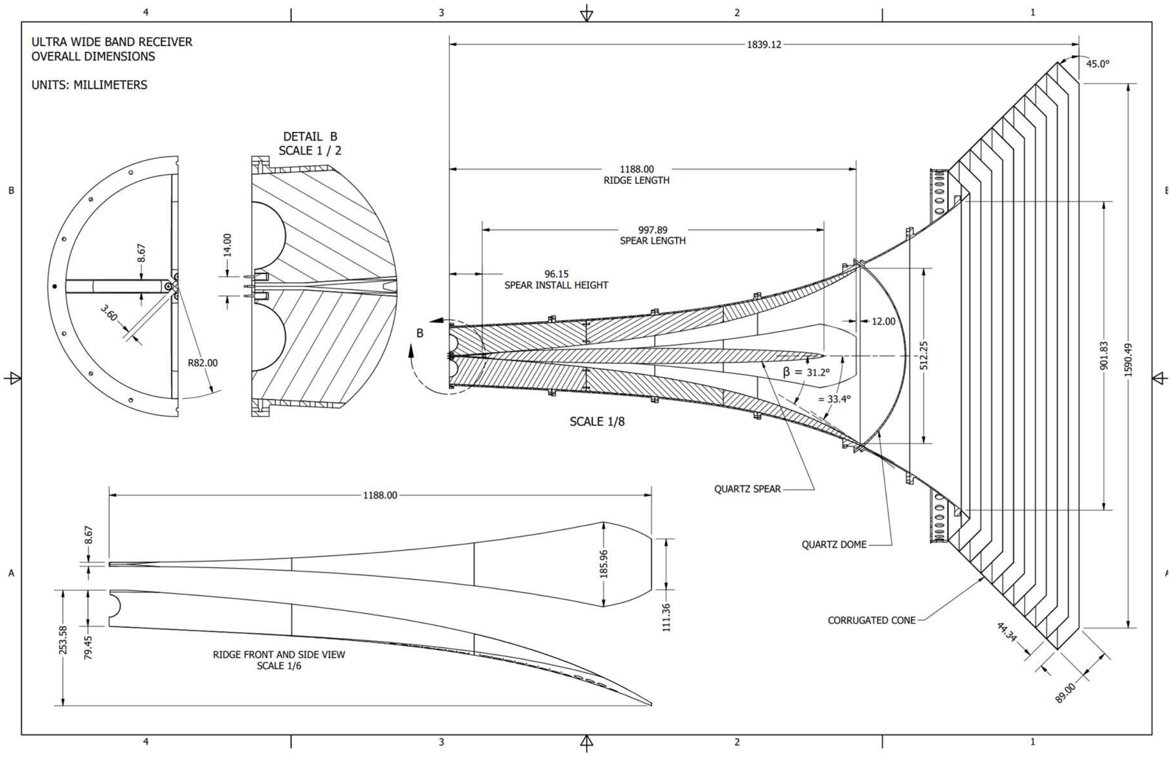

Figure 1. Mechanical Drawing of the Ultra-wide Band Feed.

Figure 2. View of the aperture at ridge end where the thermal gap is located. The quartz spear, warm section of the feed outside the dewar, and corrugation sections are not installed. The total length is 1.839m with 1.2m inside the dewar. The aperture diameter is 0.9m extended to 1.590m with addition of the courrugated cone. The input circular WG diameter is 0.164m.

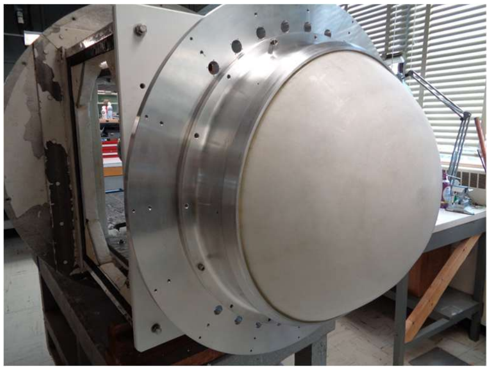

Figure 3. View with quart dome installed. The diameter is approximately 610 mm with a height of 180 mm. The center portion of the dome is 4 mm, and tapers thicker toward the rim. After the vacuum infused quartz with epoxy is cured, the dome is bonded into an aluminum ring. The dome/ring assembly is o-ring sealed against the vacuum.

	Profile	Value	Equation
1	Horn		$\mathrm{a}_y(\mathrm{z}) = h_{yi} + (h_{yo} - h_{yi})((1-A)\frac{z}{\mathrm{h\_L}} + A\left(\frac{Z}{\mathrm{h\_L}}\right)^p)$
2	Ridge Profile		$\mathrm{a}_y(\mathrm{z}) = A * (c_1 e^{Rt} + c_2) + (1-A)(\mathrm{a}_{yi} + (\mathrm{a}_{yo} - \mathrm{a}_{yi})\frac{Z}{\mathrm{r\_l}})$
3	Ridge Width		$\mathrm{a}_x(\mathrm{z}) = -rid\_w - rid\_hc(1 - e^{\left(\frac{Z}{\mathrm{r\_l}}\right)^2}$
4	c_1	10.539	$\frac{(\mathrm{a}_{yo} - \mathrm{a}_{yi})}{e^{Rr\_l} - 1}$
5	c_2	-10.539	$\frac{(\mathrm{a}_{yi}\, e^{Rr\_l} - \mathrm{a}_{yo})}{e^{Rr\_L} - 1}$
	Parameter	Value	Description
6	hyi	82 mm	Waveguide diameter probe end
7	hyo	450 mm	Waveguide diameter ridge end
8	a_{yi}	0	Ridge width input parameter (not included r_gap)
9	a_{yo}	250 mm	Ridge profile width parameter
10	A	0.8	Linear component
11	p	4	Horn profile parameter
12	h_L	1500 mm	Horn Length (not including corrugated cone)
13	R	0.0027	Ridge exponential profile parameter
14	r_gap	3.6 mm	Ridge gap
15	r_wid	4.33 mm	Ridge width initial
16	r_l	1188 mm	Ridge height
17	r_hc	130 mm	Ridge width maximum
18	β	36.71 °	Ridge flared angle $Tan^{-1}[\frac{\mathrm{A}(a_{y0} - a_{yi})\mathrm{e}^{\mathrm{Rr\_l}}}{\mathrm{e}^{\mathrm{Rr\_l}} - 1} + (1-A)\frac{(a_{y0} - a_{yi})}{r\_l}]$

Table 1. CST MWS Design Parameters.

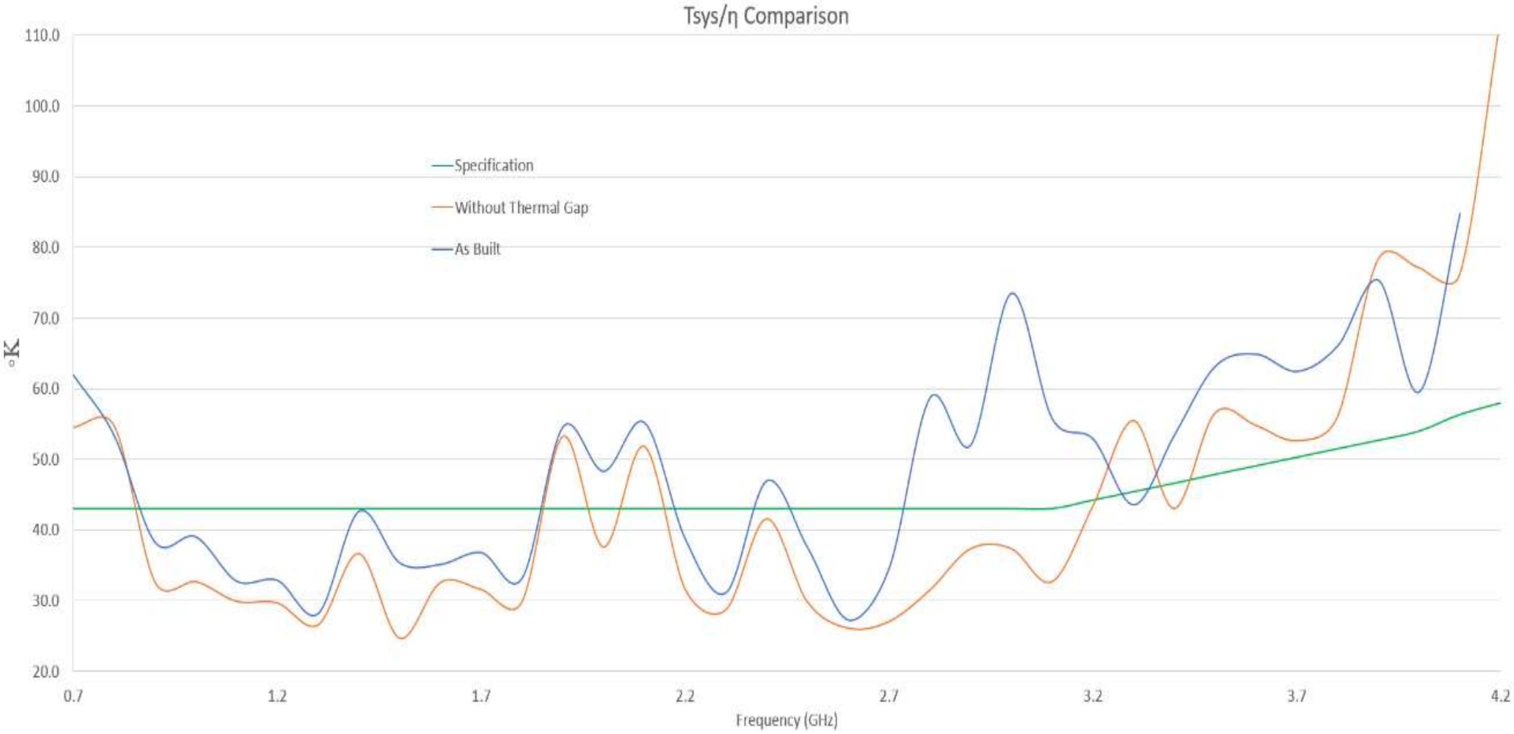

Figure 4. $\frac{T_{sys+(1-\eta_S)T_{gnd}}}{\eta_T}$. comparison from CST far fields and GRASP telescope model. The final design prediction (blue); The same model without the thermal gap (orange). A modal analysis comparison with the gap removed suggests an increase of desired modes TM12 and TE12 gives higher efficiency at 2.8 GHz.

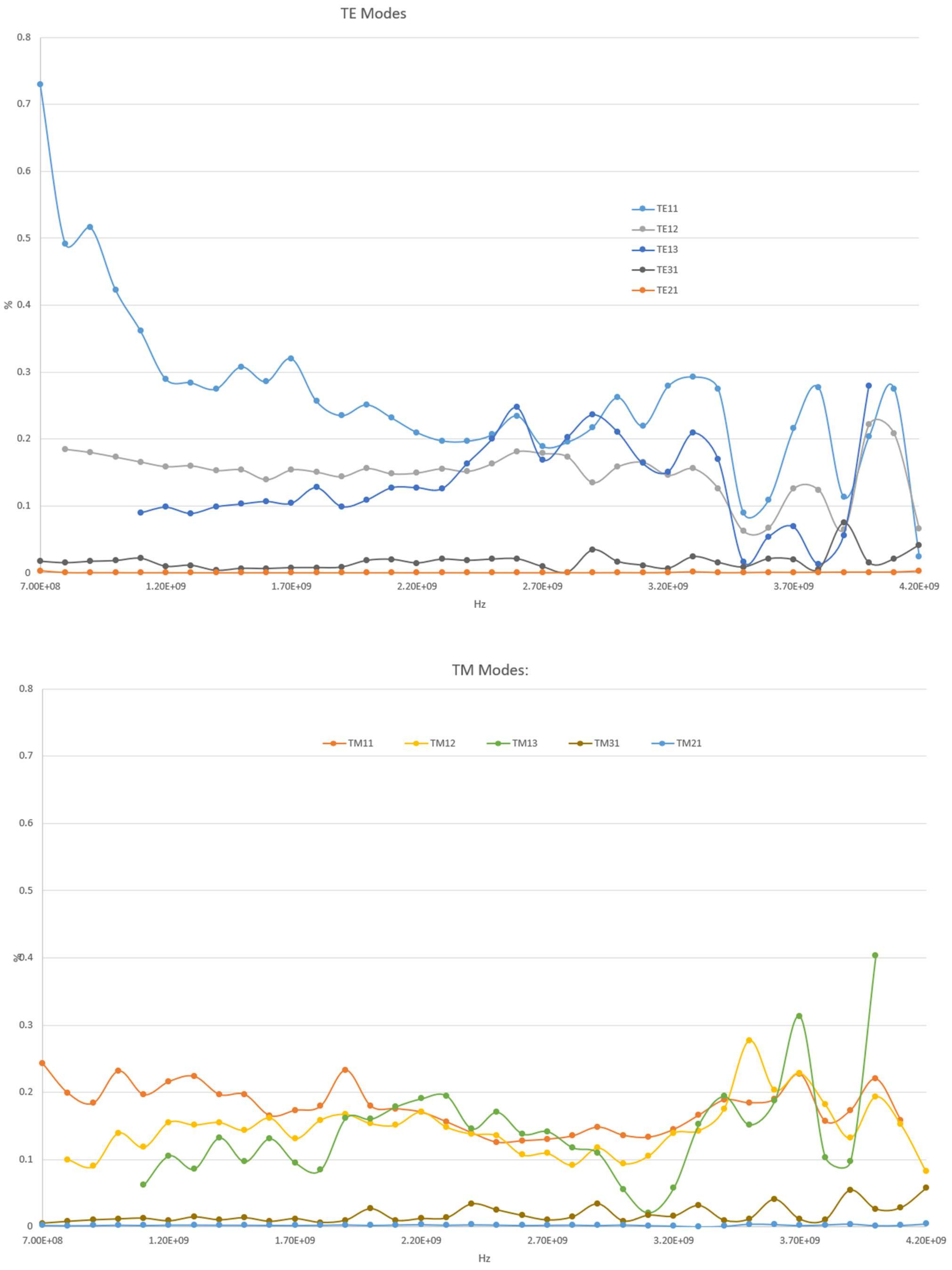

Figure 5. Calculated normalized modal content of the TE (top) and TM (bottom) modes from the CST generated far field patterns. Of note is the low TM13 content that correlates with reduced overall efficiency in Figure 6 (blue).

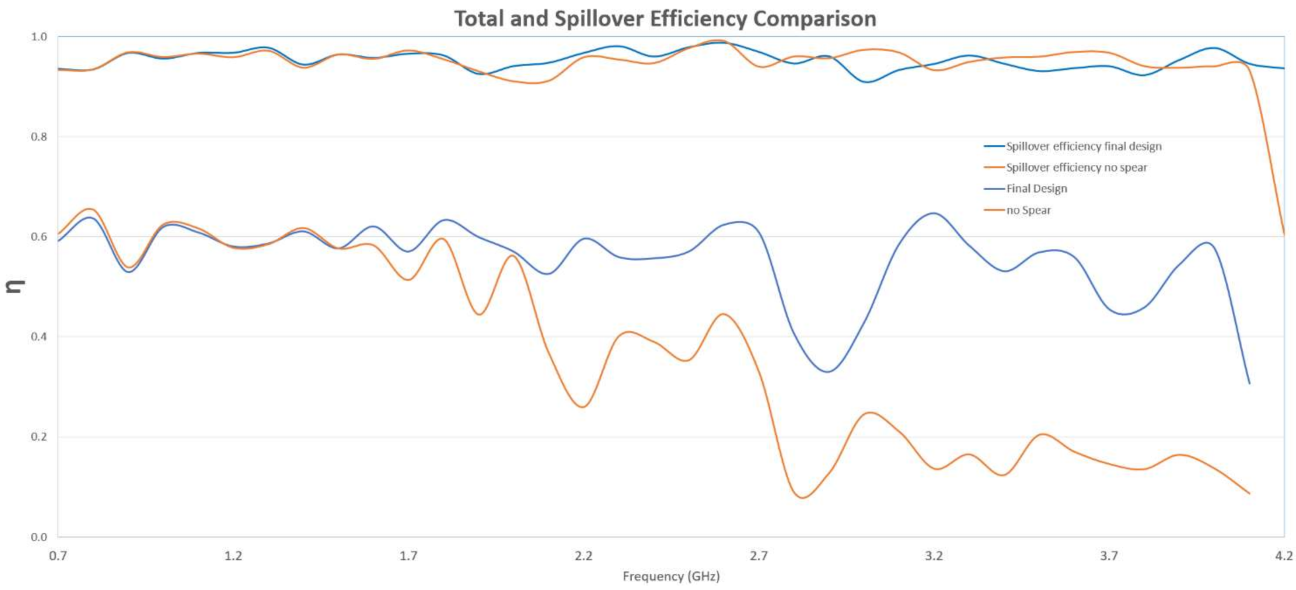

Figure 6. $\eta_{Total}\ and\ \eta_{spillover}$ comparison from CST MWS far fields and GRASP telescope model. The final design prediction (blue); The same model without the quartz spear (orange).

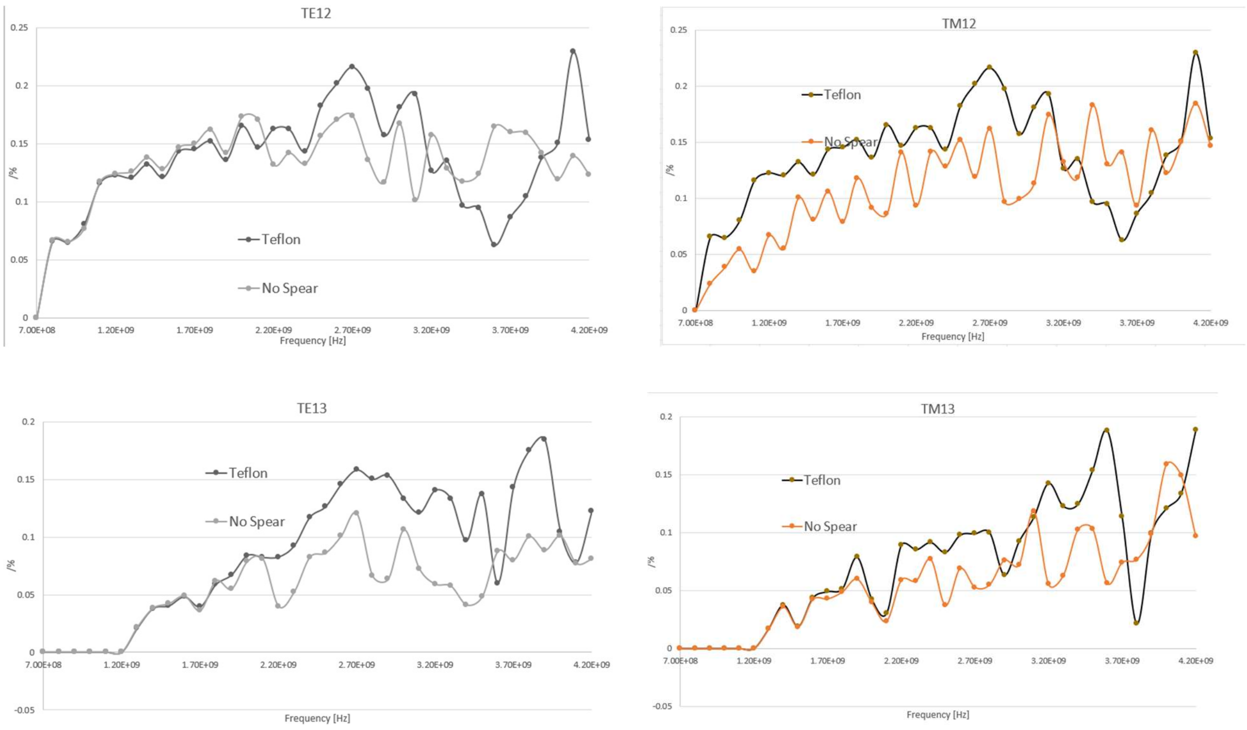

Figure 7. Calculated normalized modal content of the TE (left) and TM (right) modes from the CST MWS generated far field patterns. The reduction corresponds to a low total efficiency without a quartz spear.

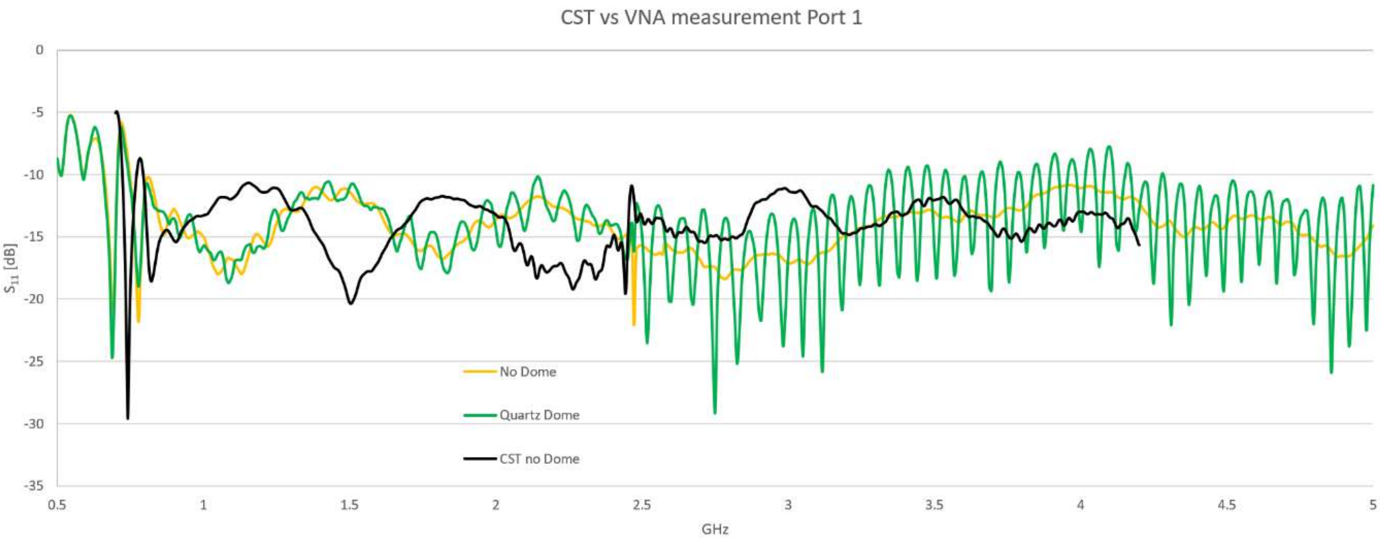

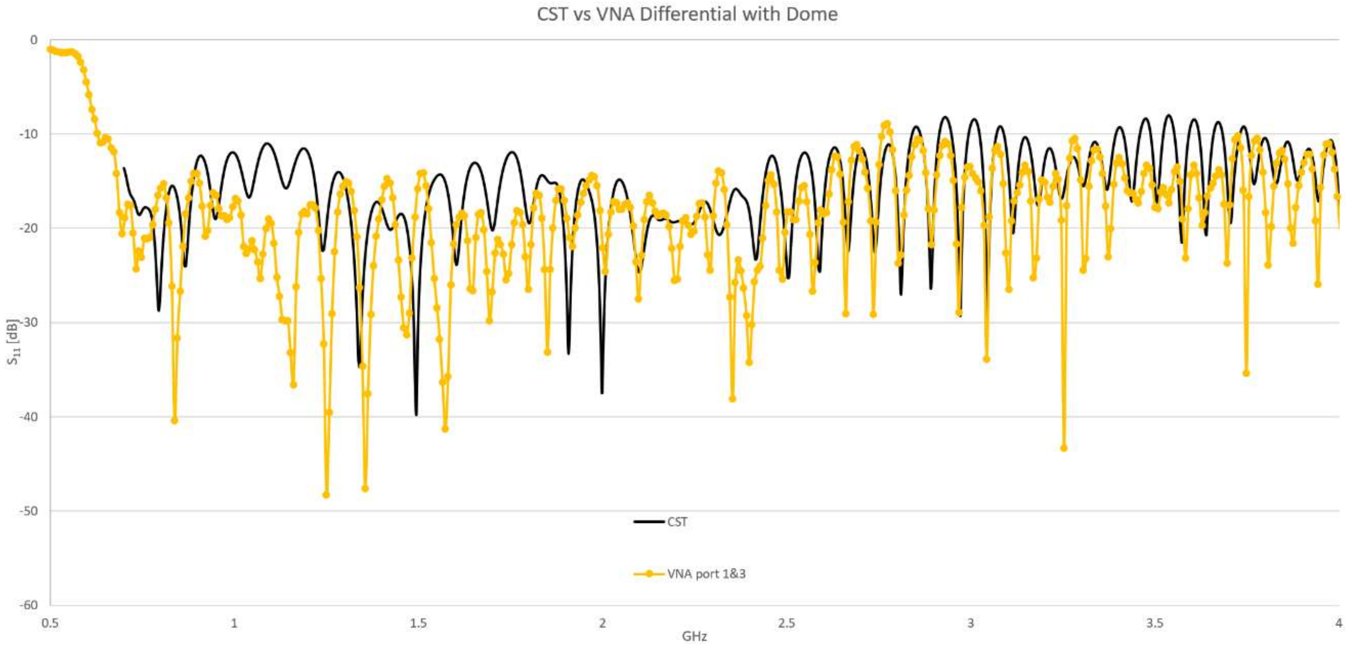

Figure 8. S parameter CST MWS model versus VNA measured reflections from the quartz dome. These measured results only include section F of the feed (no Corrugated Cone). The one port (top) and differential measurement (bottom) with Krytar Hybrid SN 214446 gives a return loss of -15.39 dB for the quartz window.

Pattern Measurements

For the characterization of far field patterns, the feed was installed on outdoor antenna range, ATR, August 2025. The results for E-plane, H-plane, and a few select cross polarization measurements are in Files:11. Calibration of amplitude and phase for diagonal feed pattern cross polarizations measurements is difficult with the current ATR software. Also, reflections from surrounding buildings distort the measured fields, thus not attempted. The CST MWO modeling results agree with the measurements in phase and amplitude with noticeable discrepancies when the higher order mode contributions are prominent above 2800 MHz. The comparisons are shown in Figure 8. Also, phase center measurements, which are time consuming, also agree with the predicted values for a few select frequencies, Files:8.

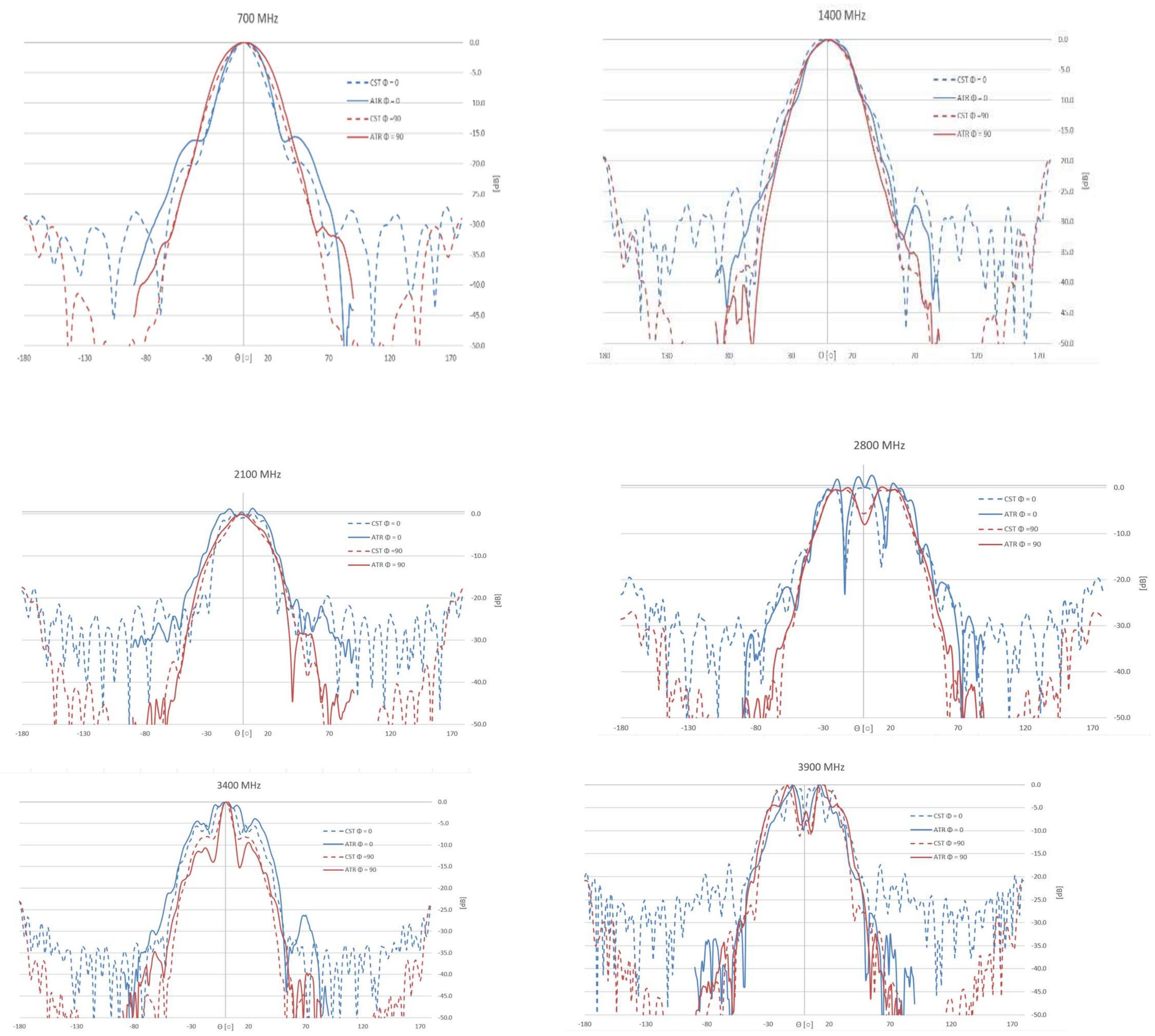

Figure 8. Comparison of the CST model predictions (dashed lines) versus the antenna range (ATR) measurements (solid lines). Both E and H plane measurements are shown.

Component Noise Temperature Measurements

Fully developed thermal and electrical models for the small Test Dewar allowed accurate testing of the low noise amplifier and 180 hybrid that comprise the differential amplifier.[7] The result shown in Figure 9 is for one of the Low Noise Factor Amplifier, LNC0.2_3A SN1520Z, and a Krytar 4005040 180-degree hybrid coupler. Two hybrids, SN214446 and SN119198 are measured together with the assumption that the noise temperature contribution from each are equal. Two additional hybrids are measured, SN191198 and SN194078, with added thermal loading to the devices to accurately raise the temperature to determine the noise temperature increase, Table 2.

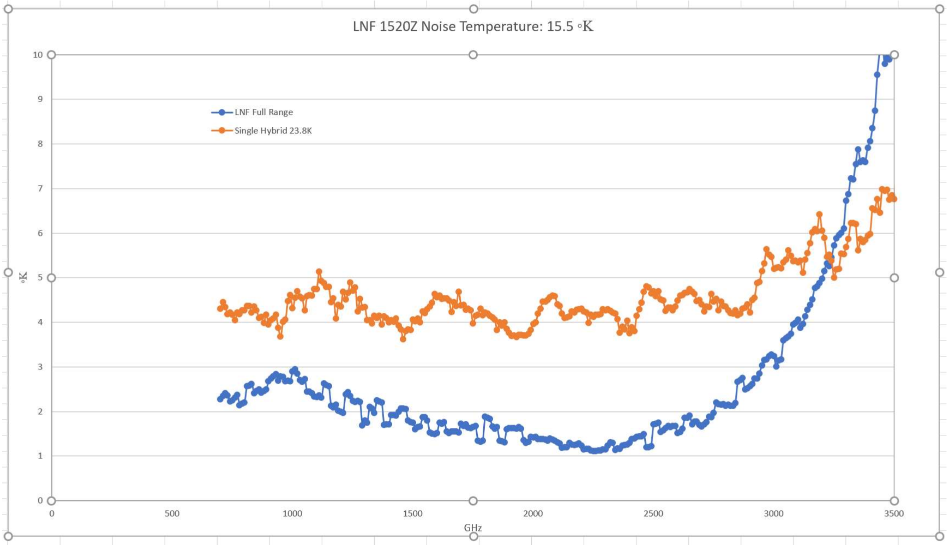

Figure 9. Noise temperature of the LNF 1520Z and the measured noise contribution one hybrid. The increase above 2500 MHz is from the UWBR IF system as the gain from the amplifier begins to decrease.

Hybrid	**Δ˚K/ΔT**
214445	0.186
214556	0.255
191198	0.114
194078	0.088
Average	0.161

Table 2. Average noise temperature increases across the band per increase in physical temperature for each hybrid. Taking the average, the expected increase in noise temperature for a 10K increase in physical temperature is 1.6 K.

Quartz Spear Dielectric Loss

With the loss tangent for fused quartz, CST MWO calculates the loss at given frequencies. A finite element analysis estimates the temperature of the spear, Files:12. With these known quantities the noise contributions can be estimated, Table 3. A similar procedure of the quartz dome along with noise temperature measurements in the Outdoor Test Range where a prototype window is placed on the ngVLA cryogenic receiver and the increase in noise temperature recorded, Figure 13 and File:13.

Freq [GHz]	CST Loss [W/m^3]	P_{in}	Loss	Tspear ◦K 200	◦K 100	◦K 60
1	0.00115	0.949609	1.0012	0.24	0.12	0.072
2	0.00495	0.97978	1.00507	1.014	0.507	0.3042
3	0.0229	0.955028	1.02461	4.922	2.461	1.4766
4	0.0313	0.964133	1.0336	6.72	3.36	2.016

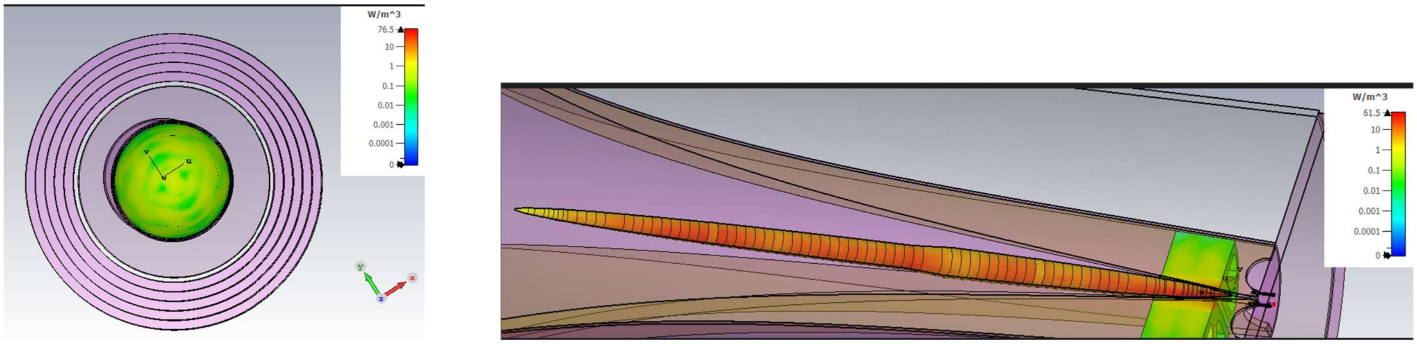

Figure 10. CST model loss of the dielectric components. The OTF quartz window measured noise temperature is shown in Figure 11.

Y Factor Temperature Measurement

The Y factor method executed in the OTF building measures the receiver noise contribution. This technique requires the absorber temperature, assumed to be 290 K ambient, and the cold load temperature composed of the CMB, galactic and atmospheric contribution, and an estimate of the ground noise pick up. The atmospheric and galactic contributions are estimated by the weather predictions of absorption, atmospheric temperature (2 GHz value), and galactic position (strongly frequency dependent) as:

$$T_{gal}(\nu) = 22.3 \left(\frac{0.408}{\nu}\right)^{2.6}$$

$$T_{cold'}(\nu) = (T_{gal} + T_{CMB})\, \mathrm{e}^{-\tau\, airmass} + T_{amb}\left(1 - \mathrm{e}^{-\tau\, airmass}\right)$$

Where T_{cmb} = 2.7, and T_{amb}= 296.75, τ = 0.008, airmass = 1.0236 taken from the weather reports at the time of measurement: https://www.gb.nrao.edu/~rmaddale/Weather/

T_{gal} depends upon the beam size and differs from the GBT measurements, but not significantly. The calculated temperature is based on the 60° beam that incorporates > 90% of the power available.

An estimate of the ground noise contribution spillover is needed for the cold sky quantity to obtain an accurate measure of receiver temperature. Given the OTF measurements are conducted with a perpendicular oriented feed, a reasonable assumption is the ground radiation is a fraction of the GBT PF spill over. Assuming a scaling factor ζ = 0.5 applied as, $T_{ground} = \zeta\, T_{spill}$, T_{Rx} can be calculated from the CST MWO and GRASP prediction of GBT spillover. A smoothing polynomial fit is applied to the predicted spillover for this analysis.

$$T_{COLD} = (T_{gal} + T_{CMB})\, \mathrm{e}^{-\tau\, airmass} + T_{amb}\left(1 - \mathrm{e}^{-\tau\, airmass}\right) + \zeta\, T_{spillover}$$

The calculated $T_{Rx}{}'$,without an estimate of T_{spill} , can be corrected with the assumed contribution factor ζ as

$$T_{Rx} = \frac{T_{ho} - Y T_{cold}{}' - Y\, \zeta\, T_{spillover}}{Y-1}$$

The OTF measured $T_{Rx}{}'$,without an estimate of T_{spill} , is corrected to give T_{Rx} and is shown in Figure 12 along with the plot of the combined noise temperature components of the receiver.

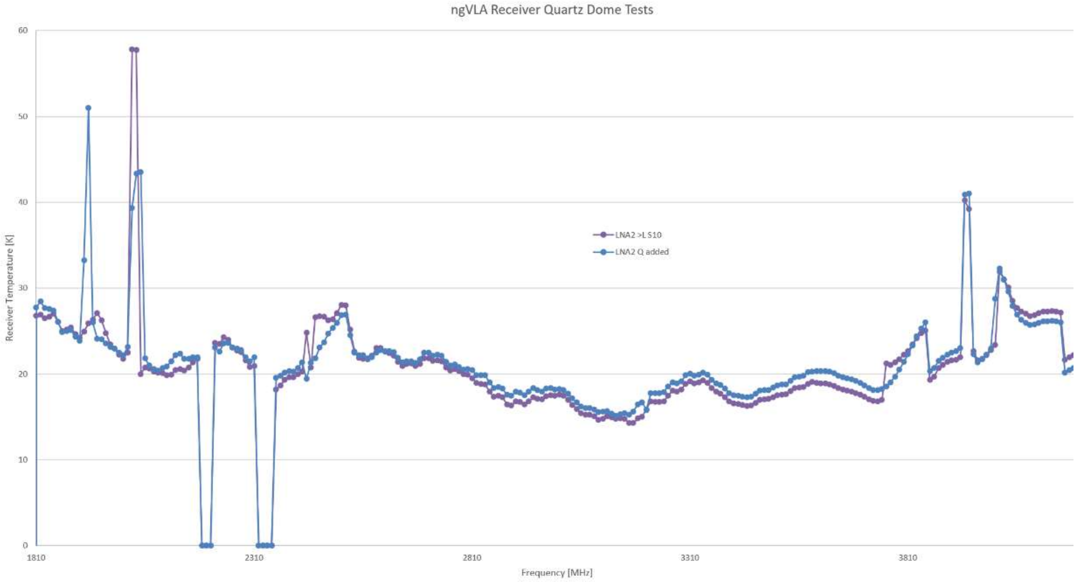

Figure 11: Quartz window tests using the ngVLA Receiver channel LNA2. An eight-inch prototype quartz window of thickness 0.026" was placed on the Mylar ngVLA window for comparison. For clarity, strong interfered data points have been removed from the raw data. The graph shows a comparison of the bare feed versus the addition of the quartz prototype. Only slight difference within the measurement variability (blue).

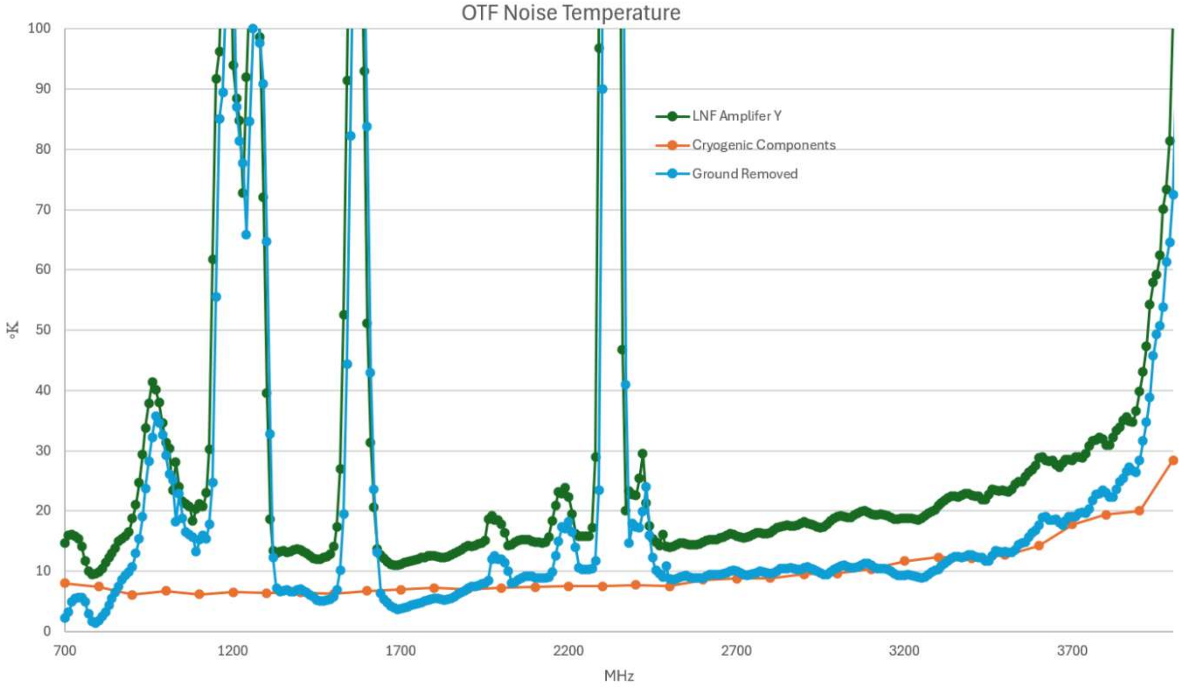

Figure 12. UWBR OTF Noise Temperature comparing the measured (green) with the corrected (blue) where the $\zeta = 0.5$ is used to correct for ground noise contribution. The orange curve is an estimate of the receiver temperature that includes all the cryogenic components both simulated and measured and the waveguide window contribution. Interference at 0.93 GHz, 1.268 GHz, 1.574 GHz, 2.195 GHz and 2.343 GHz cause the increase of measured noise temperature.

Telescope Characterization

Before the commissioning observations, the feed phase center is measured by performing focus scans on strong sources. These values then can be compared to the predicted CST MWO values. At a few select frequencies the phase center was measured on the ATR and can be found in document Files:8. The predicted versus measured values are shown in Figure 12. To compare the predicted results with the GBT observations, a system equivalent flux density is found by observing known calibrators.

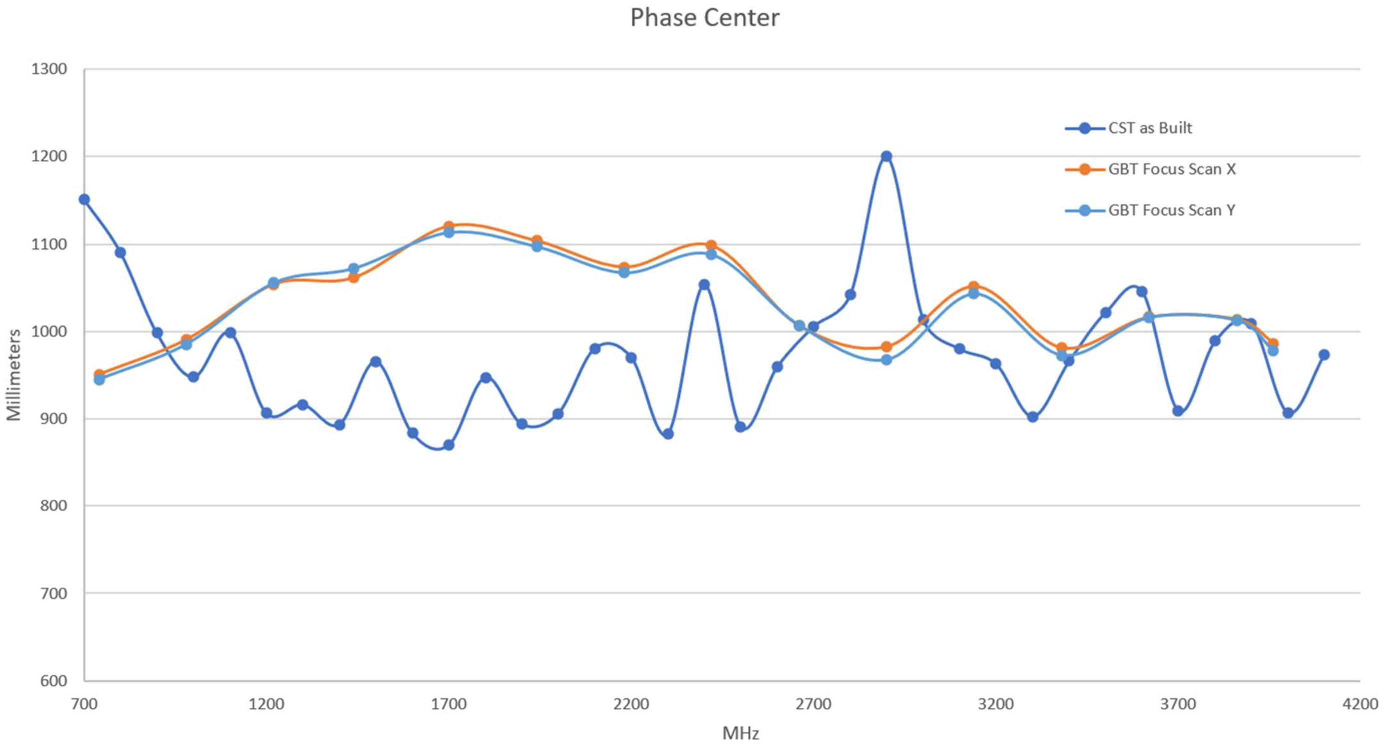

Figure 13. Phase center comparison of model prediction versus GBT commissioning results. The ordinate is referenced to the CST MWO model zero reference, which is the input waveguide flange and ridge beginning coordinate.

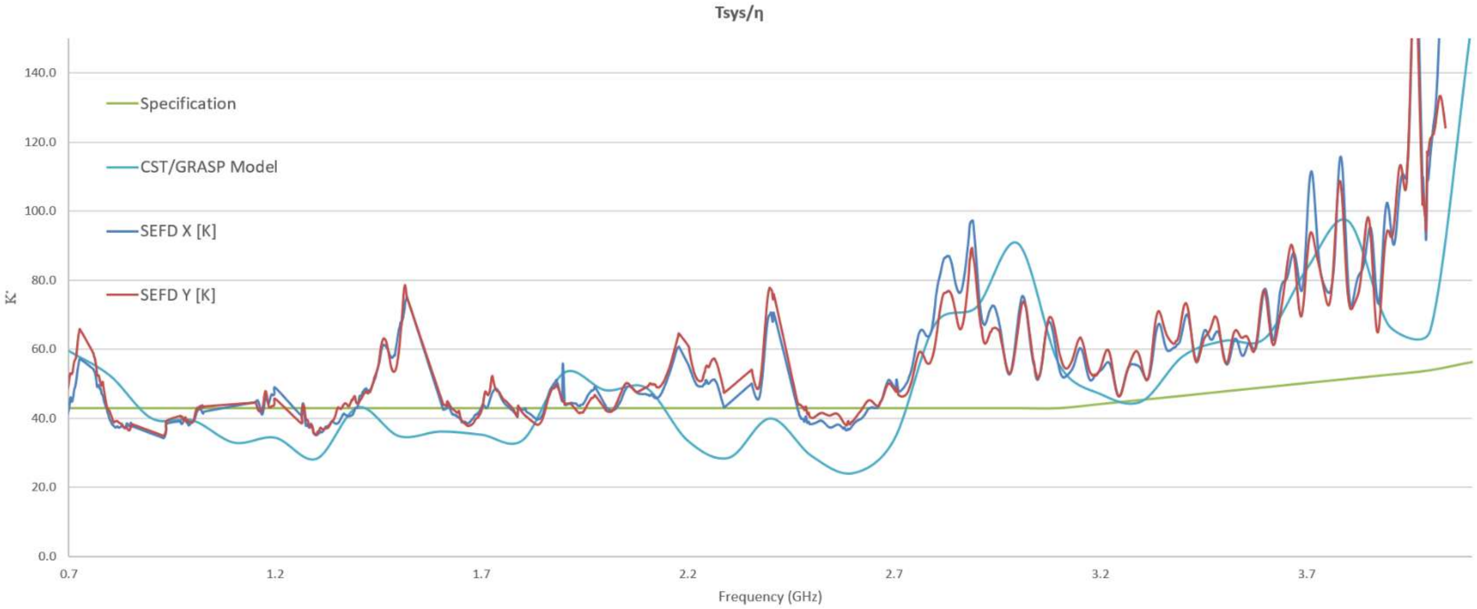

Figure 15. $\frac{T_{sys} \quad (1-\eta_S)T_{gnd}}{\eta_T}$ comparison of model prediction with average GBT commissioning results (interference removed version). The SEFD values are scaled by 2.85 to convert to Kelvin.[5] The consequences of the reduced efficiency at 2.8 GHz are a result of the distorted beam shape shown in Figure 8, although the reduction in TM13 and TE12 and corresponding increase in unwanted modes TE31 and TM31 do not exactly align.

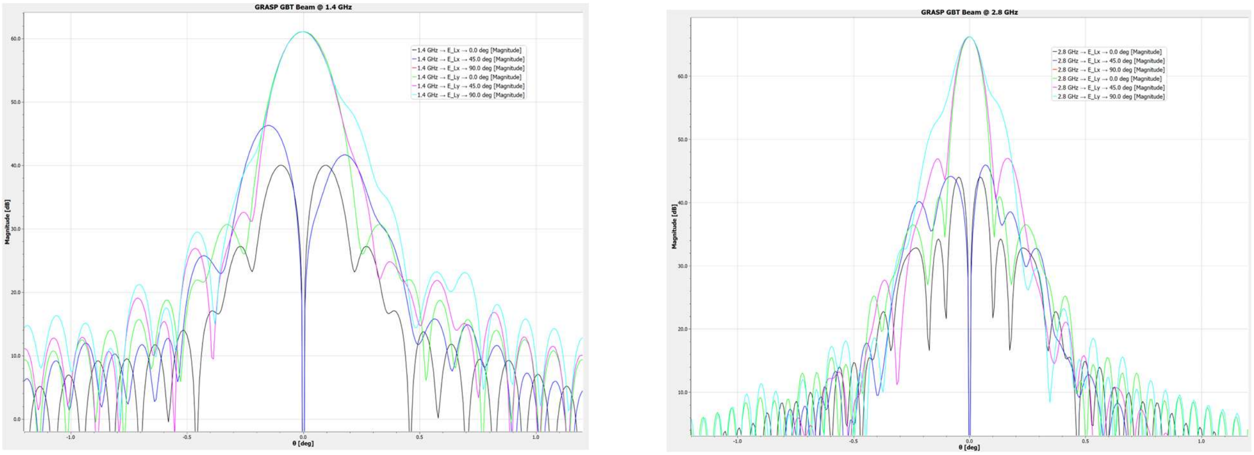

Figure 16. GRASP predictions of the far field beam using the Klahold GBT model. For GBT commissioning the beam shape was measured and a video produced compiling all the results.

Conclusion

After many years of continued effort and contrbution from scientifc, electronics, machine shop, software, and maintenance divisions, a fully commissioned scientific instrument that improves pulsar timing of the Nanograv collaboration is avaible for scientifc observations. The reciever also fills the missing coverage gap of three to four gigahertz for spectral line observations. There were many problems to solve along the journey that could have led to an unsuccessful outcome, namely the window constuction, cryogenic cooling, and ridge machining. An accurate position of the GBT primary focal point was unknown, a condition that was rectifed by comparisons of the CST MWO model, ATR measuremenst of the 800 MHz feed phase center, and focus scans with the prime focus reciever. Ultimately, the commssioned results agree and are comparable to the modeling preditions. Argueably there is some unaccounted noise contributions that were intial thought to be noise entering through the thermal gap. GBT observations and OTF noise temperature measurements with copper tape covering the gap were inconclusive, or even slightly worse, which may have casued by distoring the feed pattern. Limited GPU capabilities thrawted any attempts to optimize the feed and ridge profile with spline manipulation. There may be improvements that are comparable to eliminating the thermal gap, though the final design may not be easily machined.

Acknowledgments

This project would not have been possible without the Moore Foundation grant obtained by Scott Ransom that enabled the purchase of computing power to start modeling and start prototyping the window along with Karen O'Neil, then director, who sanctioned the effort. Ryan Lynch did most all the heavy lifting and commissioning observations, including determining the GBT focal point coordinates, and provided valuable feedback allowing ridge modification to improve performance. The machine shop, notable Phillip Doolittle and Harry Sipe, used their extensive experience to construct the feed with Pat Schaffner welding and constructing all the cone variations. Galen Watts designed built and tested the IF chain with Odroid communication hardware. Paul Marganian developed the software monitor and control system that accommodated OTF testing as well as GBT monitor and control, not to mention all the modifications to observing parameters. Art Symmes provided detailed finite element thermal analysis models for cryogenic cooling. Robert Simmons and Jonah Bausermann designed and maintained two 7.5 HP scroll compressors which provided the mass flow for running two model 1020 refrigerators. Laura Jenson and Kirstin Morin provide the reporting and valuable interference which allow us to focus on the design. Also, we would like to recognize and dedicate the completion to JD Nelson who passed away before celebrating the successful result and was a valuable team member during the process.

References

1. T.S. Beukman, “Modal-Based Design Techniques for Circular Quadruple-Ridged Flared Horn Antennas”, Phd Dissertation, University of Stellenbosch. March 2015.
2. A.H. Akgiray, “New Technologies Driving Decade-Bandwidth Radio Astronomy: Quad_Ridged Flared Horn & Compound-Semiconductor LNAs, Phd Partial Fulfillment, California Institute of Technology. April 19, 2013.
3. A. Dunning, M. Bowen, M. Bourne, D. Hayman, S.L. Smith, An Ultra-Widband Dielectrically Loaded Quad-Ridged Feed Horn for Radio Astronomy.
4. A. C. Ludwig, “Radiation Pattern Synthesis for Circular Aperture Horn Antenna”, IEEE Transactions on Antenna and Propagation”, Vol AP-14, No. 4, pp 434-440, July 1966.
5. **Title:** Sensitivity
   Authors: Wrobel, J. M. & Walker, R. C.
   Journal: Synthesis Imaging in Radio Astronomy II, A Collection of Lectures from the Sixth NRAO/NMIMT Synthesis Imaging Summer School. Edited by G. B. Taylor, C. L. Carilli, and R. A. Perley. ASP Conference Series, Vol. 180, 1999, p. 171.
   Bibliographic Code: 1999ASPC..180..171W
6. S.White, R. Simon, W. Klahold, L. Leyzorek, “GBT L-band Investigation with Physical Optics Modeling and SEFD Analysis”, GBT Memo Series 322. December 2025.
7. S.White, R. Simon, L. Leyzorek, “Test Dewar Desgin”, EDTN 233. August 2025.
8. R. Lynch, Commissioning report memos. gbfiler\uwbfeed\GBT Commissioning
9. R. Lynch, “UWB Receiver Focus Analysis”.
10. A.D. Oliver, P.J.B. Clarricoats, A.A. Kishk, and L. Shafai, Microwave Horns and Feeds, IEEE Press, 1994, ISBN 0 85296 809
11. Reflector antenna and EM modelling software | TICRA
12. https://www.3ds.com/

Files

	Path: gbfiler\doc\Archive\GBO Electronics\300008, Ultra wideband rx\Documentation\		
	Sub Path	File	Description
1	CST Models	March25_2026_Beukmanmod_AL6061angleCorr10_noQwindow_Best_noDewar_Tef_Match.cst	Final Version
2	CST Models	Jan26_2026_Beukmanmod_AL6061angleCorr10_Qwindow3p75_Best_noDewar_Tef_Match_cutout_ThrGap.cst	No Gap Model
3	CST Models	Jan29_2026_Beukmanmod_AL6061angleCorr10_Qwindow3p75_Best_noDewar_Tef_Matchadj_nospear.cst	No Spear Model
4	CST Models	July8_2024_Beukmanmod_AL6061angleCorr10_Qwindow3p75_Best_noDewar.cst	No Teflon
5	quartz and glass	Notes on choice of quartz.docx	Notes on construction
6	EXCEL	EFFICIENCY_Qwindow_GRASP.xlsx	GRASP Results
7	EXCEL	All_LNF_Krytar_IF_NoiseTempMeas.xlsm	Summary of noise contributions
8	EXCEL	UWB_August_11_2025.xlsm	August ATR FF patterns
9	EXCEL	VNA analysis.xlsm	VNA Measurement Test Dewar Components
10	EXCEL	TMTEallcorrected_2026_r450_pp.xls	Modal Analysis ridge aperture
11	EXCEL	TMTEallcorrected_2026_r795_pp.xls	Modal Analysis cone aperture
12	Thermal Model	2021-12-09_Strap+Temperature%20Sensitivity_Trades.pdf	Results
13	Quartz Dome	ngVLA_test.docx	Noise Temperature Measurement Q Dome.
14	EXCEL	receiver_performance_corrcone.xlsx	SEFD Tabulated Values
15	Inventor results	May2023 Beukman Ridges.stp	Ridge Design
16	Inventor results	May2023 Corrugations10.stp	Corrugation Design

Noise Temperature Contribution [° K]						
GHz	Spillover*	LNA+ Hybrid	Q.Spear* (70K)	Q.Window	BG+CMB	Total
0.70	18.74	7.69	0.10	0.20	8.41	39.04
0.80	19.12	7.13	0.10	0.26	6.66	37.16
0.90	9.48	5.71	0.10	0.29	5.56	25.03
1.00	12.78	6.33	0.10	0.32	4.84	28.27
1.10	9.48	5.72	0.10	0.35	4.35	23.90
1.20	9.40	5.54	0.59	0.38	4.00	23.81
1.30	6.41	5.20	0.76	0.41	3.74	20.42
1.40	16.30	5.09	0.94	0.44	3.55	30.21
1.50	10.37	4.68	1.11	0.47	3.40	23.94
1.60	12.36	4.97	1.28	0.50	3.29	26.30
1.70	9.90	4.98	1.46	0.53	3.20	24.06
1.80	10.91	5.05	1.63	0.56	3.13	25.28
1.90	21.72	4.66	1.80	0.59	3.07	35.83
2.00	17.14	4.66	1.98	0.62	3.02	31.41
2.10	15.21	4.60	2.15	0.65	2.98	29.59
2.20	9.46	4.52	2.32	0.68	2.94	23.93
2.30	5.50	4.32	2.49	0.71	2.92	19.94
2.40	11.59	4.32	2.67	0.74	2.89	26.21
2.50	6.15	3.92	2.84	0.77	2.87	20.55
2.60	3.56	4.75	3.01	0.80	2.85	18.98
2.70	8.86	4.81	3.19	0.83	2.84	24.52
2.80	15.62	4.68	3.36	0.86	2.83	31.35
2.90	11.46	5.10	3.53	0.89	2.81	27.79
3.00	26.37	5.02	3.71	0.92	2.80	42.82
3.10	19.40	5.49	3.88	0.95	2.80	36.51
3.20	15.91	6.65	4.05	0.98	2.79	34.37
3.30	10.97	7.11	4.23	1.01	2.78	30.10
3.40	15.77	6.77	4.40	1.04	2.77	34.74
3.50	20.05	7.02	4.57	1.07	2.77	39.47
3.60	18.36	8.37	4.74	1.10	2.76	39.34
3.70	17.24	11.75	4.92	1.13	2.76	41.80
3.80	22.44	13.14	5.09	1.16	2.75	48.58
3.90	13.56	13.55	5.26	1.19	2.75	40.32
4.00	6.54	21.81	5.44	1.22	2.75	41.76

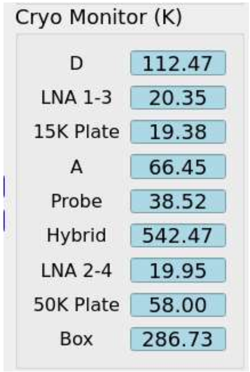

Cryo Monitor (K)

D	112.47
LNA 1-3	20.35
15K Plate	19.38
A	66.45
Probe	38.52
Hybrid	542.47
LNA 2-4	19.95
50K Plate	58.00
Box	286.73

Table 3. All Noise Components for $\frac{T_{sys+(1-\eta_S)T_{gnd}}}{\eta_T}$ calculation. * Spillover and quartz spear contributions are attributed to CST MWO and Anysys thermal models. Typical cryogenic temperatures for measured results.